MASKE: Particle-Based Chemo-Mechanical Simulations of Degradation Processes

Enrico Masoero(✉)

School of Engineering, Cardiff University, Cardiff, UK
masoeroe@cardiff.ac.uk

Abstract. The long-term performance of new cementitious materials is uncertain. To help predict durability and manage uncertainty, the models must capture the fundamental mechanisms driving degradation in new binders. Such mechanisms evolve slowly and are strongly chemo-mechanically coupled, all of which challenges the existing simulations. This article presents MASKE: a simulator of microstructural evolution based on interacting particles, which represent multiphase solid domains in an implicit ionic solution. Chemical reactions, sampled through Kinetic Monte Carlo to reach long time scales, determine precipitation/dissolution processes whose rates depend on solution chemical potentials and on particle interaction energy. Published results from MASKE have already addressed aggregation-driven precipitation of C-S-H nanoparticles, stress-driven dissolution of C_3S crystals at screw dislocations, and carbonation of calcium hydroxide in a C-S-H matrix. Here new results are presented, focussing on a nanocrystal of calcium hydroxide and discussing: (i) its chemical equilibrium and dissolution/growth kinetics in stress-free conditions, and (ii) the emergence of pressure-solution and crystallization pressure when the crystal is compressed between platens. Similar chemo-mechanical processes contribute to important degradation modes of concrete, such as creep, sulphate attack, and alkali-silica reaction.

Keywords: Simulation · Degradation · Dissolution and growth · Pressure solution · Crystallization pressure

1 Introduction

The current environmental targets are putting the concrete industry under pressure to reduce its carbon emissions [1]. Part of the solution is to transition to less CO_2 intensive cements, such as LC^3 and other alkali activated binders [2]. However, the long-term performance of these new binders is largely unknown, and there is documented risk that accelerated aging tests may not trigger representative mechanisms of slower degradation during service [3–5]. Modelling and simulation can support the transition, by providing a fundamental understanding of the degradation mechanisms in new materials, thus informing better extrapolations of short-term results to long time scales.

Concrete degradation is underpinned by chemical reactions at the nanoscale and deformation at the microscale. At the nano-to-micro scale, free energy changes from

© The Author(s), under exclusive license to Springer Nature Switzerland AG 2023
A. Jędrzejewska et al. (Eds.): SynerCrete 2023, RILEM Bookseries 43, pp. 159–170, 2023.
https://doi.org/10.1007/978-3-031-33211-1_15

chemical reactions and mechanical stress are comparably large, hence strongly coupled chemo-mechanical processes emerge. Two examples are: (i) stress-driven dissolution, causing non-linear dissolution vs. supersaturation curves in various minerals [6] and contributing to creep deformations [7] (along with its dual process of dissolution-driven stress relaxation which also contributes to creep [8, 9]); (ii) crystallization pressure [10], underpinning degradation processes such as freeze-thaw, alkali-silica reactions, and delayed ettringite formation. Chemo-mechanical coupling is captured by ab-initio and atomistic simulations, but these are limited to length and time scales that are too small to address the degradation of concrete. At the nano-to-micro mesoscale, particle-based simulations have coarse-grained the results of atomistic simulations into potentials of mean force, used for studying mechanical processes directly at the mesoscale [11]. However, chemical evolution in particle-based simulations has been either neglected or oversimplified, which is a limitation for the degradation processes in concrete.

This article adopts MASKE: a particle-based simulator of chemo-mechanical evolution at the nano-to-micro mesoscale, in complex mineral systems within a co-evolving ionic solution. A precursor of MASKE was used in 2017 to simulate precipitation of coarse-grained C-S-H nanoparticles [12], showing how both mechanical aggregation and solution saturation contribute to the early hydration rate curve of Portland cement. In its current version, except slightly different rate equations, MASKE was used in 2020 to simulate the dissolution of a C_3S crystal, where each particle represented one C_3S molecule [13]. Focussing on a high-stress intersection between a screw dislocation and the mineral surface, the simulations predicted the experimentally observed sigmoidal dependence of the dissolution rate on the solution supersaturation. Finally, MASKE was recently used to simulate carbonation, i.e. precipitation of $CaCO_3$ particles in a system of dissolving calcium hydroxide and C-S-H, both modelled at the molecular scale (1 particle = 1 molecule) and in contact with an aqueous solution rich in CO_3^{-2} [14].

This article starts with an overview of the MASKE simulator in its current version, presenting its Kinetic Monte Carlo approach that allows sampling long timescales, and the rate equations for dissolution and precipitation events. The explanation is targeted to simulations with only one mineral species, $Ca(OH)_2$ (called CH), where each particle represents one molecule. The system is parametrized for CH, including potentials of mechanical interaction between particles and thermodynamic and kinetic parameters that control the dissolution and precipitation reactions. A spheroidal nanocrystal is then built from an orderly agglomeration of CH particles. The crystal is first studied in stress-free conditions, predicting the mechanisms and rates of dissolution and growth at various levels of solution saturation, determined by the concentrations of Ca_{2+} and OH^- ions in solution. Then two steel platens are added to compress the crystal at pressures between 10 and 90 MPa. With this added mechanical stress, the simulations capture the buildup of creep deformations from pressure-induced dissolution, as well as the swelling of the system when a high solution saturation drives strong crystallization.

2 Methodology

2.1 The MASKE Simulator

MASKE is a C++ code to simulate the kinetic evolution of microstructures featuring multiple solid phases in a fluid medium. The fluid is described by the average concentrations of chemical species in it, e.g. water and ions. The solids are modelled as spherical particles that interact mechanically through effective potentials: Fig. 1. One particle may be as small as a single molecule (as in this article) or it may coarse-grain thousands or millions of molecules. An implicit additional volume of solution ΔV_{sol} can also be attached to the simulation box, to allow for solution buffering when needed.

The evolution of the system is driven by continuous and discrete events, which MASKE places onto a common timescale. Continuous events are integrated over time with user-assigned time step; examples may be diffusion equations or equations of motion. This article will not consider continuous events but only discrete events, for which there is a time lag Δt between two events. Examples are the precipitation or dissolution of a solid particle, which also alter the solution by consuming or releasing ions. Δt is not assigned a priori and it typically changes during a simulation, depending on the evolving composition of the solution and mechanical interactions between particles.

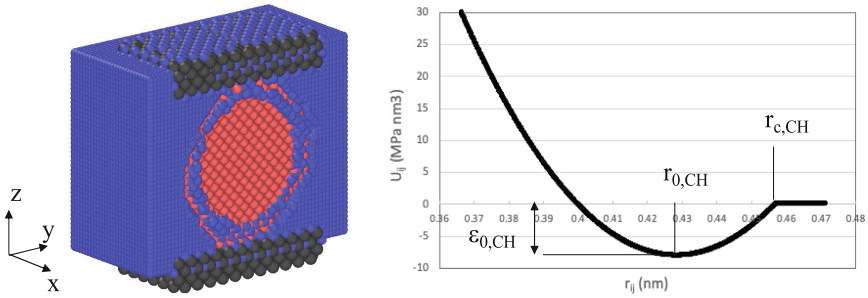

Fig. 1. Left: a typical simulation snapshot (using OVITO [15]) with steel platen particles in grey, a crystal of real $Ca(OH)_2$ particles for dissolution in red, and trial $Ca(OH)_2$ particles for precipitation in blue. Right: harmonic interaction potential between pairs of $Ca(OH)_2$ particles.

MASKE uses off-lattice rejection-free Kinetic Monte Carlo (KMC) to compute the Δt until the next discrete event. First a list of possible discrete events is created, e.g. dissolution of N existing particles and precipitation of a new particle at M possible sites. Each possible event is given a rate R_i and the KMC algorithm computes Δt as:

$$\Delta t = \frac{1}{\sum_{i=1}^{N+M} R_i} \cdot \ln\left(\frac{1}{u}\right) \tag{1}$$

u is a random number uniformly distributed between 0 and 1. An event is selected with probability proportional to its R_i and carried out. The rates R_i depend on the chemical reactions driving the events, for which the user must provide stoichiometries and thermodynamic and kinetic parameters. The rates also depend on the underlying

mechanisms, e.g. classical rather than nonclassical nucleation, growth and dissolution. In this article, since each particle will represent only one solid molecule, Transition State Theory (TST) will be the starting point to express the dissolution and precipitation rates.

The precipitation rate of a unimolecular particle in MASKE is:

$$r_p = \frac{k_B T}{h c^{\ddagger} \gamma^{\ddagger}} \exp\left(-\frac{\Delta G_p^{\ddagger}}{k_B T}\right) Q_{r,p} \Delta \mathrm{V} \cdot V_t^{-\alpha/3} = k_p Q_{r,p} \Delta \mathrm{V} \cdot V_t^{\alpha/3-1} \tag{2}$$

k_p is the rate constant of the precipitation reaction; MASKE explodes it into its parts to capture the effect of temperature T on the rates. This brings in the Boltzmann k_B and Planck h constants and the activity coefficient $\gamma^{\ddagger}$, concentration $c^{\ddagger}$, and activation energy $\Delta G_p^{\ddagger}$ of the activated complex for precipitation in standard state. $\Delta G_p^{\ddagger}$ can be obtained from experiments at different T, but its value depends on the arbitrary choice of $c^{\ddagger}$, hence the two parameters must be provided consistently. $Q_{r,p}$ is the activity product of the n_r molecules in solution, with concentrations c_i, that react to form the solid:

$$Q_{r,p} = \prod_{i=1}^{n_r} \gamma_i c_i \tag{3}$$

The activity coefficients γ_i are computed using a version of the Debye-Hückel theory that accounts also for uncharged molecules and concentrated electrolytes:

$$\log_{10}(\gamma_i) = \frac{-z_i^2 A \sqrt{I}}{1 + B a_i \sqrt{I}} + b_i \sqrt{I} \tag{4}$$

z_i is the charge of the i^{th} molecule, A and B are solvent-specific constants (0.51 and 3.29 nm^{-1} for water), a_i is the hydrated radius of the molecule in solution, b_i is a molecule-specific constant, and I is the ionic strength of the fluid with all its n_s species:

$$I = \sum_{i=1}^{n_s} c_i z_i^2 \tag{5}$$

To sample precipitation events, MASKE creates a lattice of trial particles with a user provided geometry, e.g. the cubic lattice in Fig. 1. ΔV in Eq. (2) is the volume of one lattice cell. The trial particles are assigned the same interaction potentials as the corresponding species of real particles, and then the total interactions energy of the system is minimized while keeping all real particles fixed in their positions. This moves each trial particle to the most favourable precipitation site close to it (note the off-lattice nature of this operation). All the trial particles within the same attractive basin of a given set of real particles will ultimately move to the same local energy minimum, i.e. the same site. This implies that, for an infinitely fine sampling lattice with $\Delta V \to 0$, the sum in Eq. (1) eventually attributes a cumulative volume weight V_t to the generic precipitation site, with Vt being the volume of the attractive interaction basin surrounding the site. Therefore, the overall r_p in Eq. (1) associated to the site will eventually scale as $V_t^{\alpha/3}$, where α is the spatial dimension of $c^{\ddagger}$. $\alpha = 3$ if $c^{\ddagger}$ is per unit volume and $\alpha = 2$ if $c^{\ddagger}$ is per unit surface; the latter is typical for dissolution and precipitation processes. All in all, the units of r_p in Eq. (1) are correctly number of events per unit time.

The dissolution rate of a unimolecular particle in MASKE is:

$$\begin{aligned} r_d &= \frac{k_B T}{h c^{\ddagger} \gamma^{\ddagger}} \exp\left(-\frac{\Delta G_d^{\ddagger}}{k_B T}\right) \exp\left(-\frac{\Delta U_d - \Delta U_k}{k_B T}\right) Q_{r,d} V_t^{\alpha/3} \\ &= k_d \exp\left(-\frac{\Delta U_d - \Delta U_k}{k_B T}\right) Q_{r,d} V_t^{\alpha/3} \end{aligned} \tag{6}$$

$\Delta G_d^{\ddagger}$ is the standard state activation energy of the dissolution reaction, k_d its reaction constant, and $Q_{r,d}$ the activity product of the molecules reacting to dissolve the solid. V_t is the volume of the attraction basin surrounding the particle that is being sampled for dissolution. The second exponential term in Eq. (6) is new and it features the dissolution-induced change in (position-dependent) excess free energy of a particle ΔU_d, minus the same energy change for a stress-free particle occupying a kink position in a crystal lattice ΔU_k. The rationale for this term is that adding or removing a stress-free particle in kink position should not alter the free energy of the solid. Particles that are less connected than a kink or under mechanical stress will be in a higher energy state than a kink, hence their dissolution would entail a $\Delta U_d - \Delta U_k < 0$ and thus a greater rate than better-connected, less stressed particles.

The above rate equations may be used directly to sample precipitation and dissolution, but this may lead to inefficient simulations, with many precipitation events at energetically unfavourable locations, as r_p in Eq. (2) is position-independent, immediately followed by fast dissolution. A way to avoid such fluctuations is to employ net rates:

$$r_d^{net} = r_d - r_{d-} = \frac{k_B T}{h c^{\ddagger} \gamma^{\ddagger}} \exp\left(-\frac{\Delta G_d^{\ddagger}}{k_B T}\right) \left[\exp\left(-\frac{\Delta U_d - \Delta U_k}{k_B T}\right) Q_{r,d} - \frac{Q_{p,d}}{K_{eq,d}}\right] V_t^{\alpha/3} \tag{7}$$

$$r_p^{net} = r_p - r_{p-} = \frac{k_B T}{h c^{\ddagger} \gamma^{\ddagger}} \exp\left(-\frac{\Delta G_p^{\ddagger}}{k_B T}\right) \left[Q_{r,p} - \exp\left(-\frac{\Delta U_d - \Delta U_k}{k_B T}\right) \frac{Q_{p,p}}{K_{eq,p}}\right] \Delta V \cdot V_t^{\alpha/3-1} \tag{8}$$

r_{d-} in Eq. (7) is the backward reaction for dissolution, whose expression is analogous to r_p in Eq. (2). Therefore r_{d-} brings in the activity product of the products of dissolution, $Q_{p,d}$. The equilibrium constant $K_{eq,d}$ of the dissolution reaction emerges because $\Delta G_p^{\ddagger} = \Delta G_d^{\ddagger} + RT \ln(K_{eq,d})$. Analogous considerations apply to Eq. (8), where r_{p-} is the backward precipitation reaction, $Q_{p,p}$ is the activity products of the products of precipitation, and $K_{eq,p}$ is the equilibrium constant of the precipitation reaction. Equations (7) and (8) apply to simple, one-step, unimolecular reactions, but richer rate expressions could be used instead to capture more complex reaction mechanism e.g. coarse-grained rates in [12].

2.2 The Calcium Hydroxide System in This Article

This article will apply MASKE to simulate the dissolution and precipitation of a nanocrystal of calcium hydroxide, $Ca(OH)_2$ (or CH in cement notation), with externally applied forces, in a aqueous solution of Ca^{2+} and OH^- ions. CH was chosen as an

example to demonstrate the capabilities of MASKE, without targeting processes that are technologically impactful for this mineral specifically. Indeed, CH was chosen because it is simple and its kinetic and thermodynamic parameters are established in the literature.

The nanocrystal is described as a cluster of individual spherical particles arranged in a face centred cubic (FCC) lattice: see Fig. 1. Each particle represents one CH molecule with volume $v_{m,CH} = 0.05567\ nm^3$, which gives a particle diameter $D_{CH} = 0.4737$ nm. Pairs *i,j* of particles at a distance r_{ij} interact through a harmonic potential (see Fig. 1):

$$U_{ij,CH}(r_{ij}) = \begin{cases} \frac{1}{2}k_{ij,CH}\left(r_{ij} - r_{0,CH}\right) - \varepsilon_{0,CH} & \text{if } r_{ij} \le r_{c,CH} \\ 0 & \text{if } r_{ij} > r_{c,CH} \end{cases} \tag{9}$$

$r_{0,CH} = 0.74^{1/3}\ D_{CH} = 0.4285$ nm is the equilibrium distance, with correction to remove the artificial porosity of 0.26 introduced by the FCC arrangement (more details in [13]). $K_{ij,CH} = E_{CH}\ \pi D_{CH}^2/\left(4\ r_{0,CH}\right)$ is the interaction stiffness, with $E_{CH} = 48$ GPa the Young modulus of CH [16]. The bond energy at equilibrium is set to $\varepsilon_{0,CH} = \gamma_{CH}\ \pi D^2/6$ (see rationale in [13]), where $\gamma_{CH} = 68.4\ mJ/nm^2$ is the CH-water interfacial energy [17]. $r_{c,CH}$ the interaction cut-off, set to when U_{ij} returns to 0 at $r_{ij} > r_{0,CH}$, which leads to $r_{c,CH} = 0.4571$ nm and therefore to a bond failure strain $(r_{c,CH}/r_{0,CH} - 1) = 7.2\%$.

Particle dissolution and precipitation follow the reaction:

$$Ca(OH)_2 \rightleftharpoons Ca^{2+} + 2OH^- \tag{10}$$

with $K_{eq,d} = 6.30866 \cdot 10^{-6}$ [18] (and therefore $K_{eq,p} = K^{-1}{}_{eq,d} = 1.585125 \cdot 10^5$). The net rates follow Eqs. (7) and (8), with $\gamma^{\ddagger} = 1$ as typical in reactions involving [19], $\Delta G_d^{\ddagger} = 74$ kJ/mol for a $c^{\ddagger} = 1\ \mu$ mol/m^2 (so $\alpha = 2$) as per rate constant in [20], hence $\Delta G_p^{\ddagger} = \Delta G_d^{\ddagger} + RT \ln(K_{eq,d}) = 44.6$ kJ/mol. The activity coefficients of the Ca^{2+} and OH^- follow Eq. (4) with $a_{Ca} = 0.486$ nm, $b_{Ca} = 0.15$, $a_{OH} = 1.065$ nm and $b_{OH} = 0.064$ [18]. In all cases, the reactant of the dissolution reaction as well as the product of precipitation is just solid CH, hence $Q_{r,d} = Q_{p,p} = 1$. $U_{kink} = \gamma_{CH}\ \pi D^2$ as per rationale in [13]. V_t is approximated as to $v_{m,CH}\ r_{c,CH}/r_{0,CH}$. Precipitation is sampled using a cubic lattice of trial particles (Fig. 1) with linear cell size of $r_{0,CH}/2$, leading to $\Delta V = 0.00984\ nm^3$.

A spheroidal nanocrystal is first obtained starting from a cubic FCC crystal of linear size 10 $r_{0,CH}$ and placing it in an undersaturated solution with $c_{Ca} = 15$ mmol/L: see Fig. 2a. A large buffer solution volume $\Delta V_{sol} = 10^{24}\ nm^3$ is added, so any dissolution has negligible impact on the concentrations of ions in solution. Only Ca and OH ions are assumed to populate the solution (which is an oversimplification for future improvements), so in all cases in this article $c_{OH} = 2\ c_{Ca}$. Therefore, this initial dissolution phase was conducted at saturation index $\beta = Q_{r,p}/K_{eq,d} = 0.786$, as per Eqs. (3)-(5), where $\beta < 1$ indicates an undersaturated solution in which the crystal should dissolve.

The spheroidal crystal is then tested for stress-free dissolution and precipitation by running a set of MASKE simulations, each with a different level of c_{Ca} (and thus c_{OH}) to impose β values between 0 and 10 (c_{Ca} between 0 and 39.1 mmol/L), always with $\Delta V_{sol} = 10^{24}\ nm^3$ to fix the concentrations. Chemical equilibrium is expected at $\beta = 1$.

The next simulation campaign starts with two added steel (S) platens, one above and one below the CH crystal, discretized using spherical steel particles on an FCC lattice:

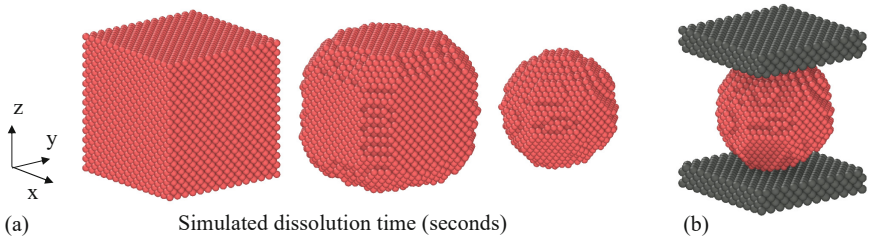

Fig. 2. (a) Creation of a spheroidal $Ca(OH)_2$ nanocrystal by dissolution of an initially cubic one at saturation index $\beta = 0.786$. (b) Addition of steel platens to apply stress along Z.

see Fig. 2b. The steel particles interact with each other through a potential analogous to Eq. (9), with parameters: $D_S = 0.6$ nm (arbitrary), $r_{0,S} = 0.74^{1/3}\ D_S = 0.5427$ nm, $k_{ij,S} = E_S\ \pi D^2_S/(4\ r_{0,S})$ with $E_S = 200$ GPa, $\varepsilon_{0,S} = \gamma_S\ \pi D^2/6$ with $\gamma_S = 200$ mJ/nm^2 (arbitrarily set just to create stronger bonds than in CH), $r_{c,S} = 0.5614$. The platens are not allowed to dissolve or precipitate: they will just apply mechanical stress to the CH crystal. To this end, a purely repulsive Hookean potential is set between CH and steel particles: $U_{ij,CH\text{-}S} = ½\ k_{ij,CH\text{-}S}\ (r_{ij} - r_{0,CH\text{-}S})$ for $r_{ij} \leq r_{0,CH\text{-}S}$, and $U_{ij,CH\text{-}S} = 0$ for $r_{ij} > r_{0,CH\text{-}S}$, with $k_{ij,CH\text{-}S} = 2\ [2\ k_{ij,CH}\ 2\ k_{ij,S}\ /(2\ k_{ij,CH} + 2\ k_{ij,S})]$ and $r_{0,CH\text{-}S} = ½\ (r_{0,CH} + r_{0,S})$. All the particles in the platen below the CH crystal are fixed in position, whereas the upper platen is fixed on the horizontal XY plane and free to move vertically along Z. A vertical downward force f_Z is applied to each of the 1,058 particles of the upper platen, whose horizontal area is $(16\ r_{0,S})^2$, hence the vertical pressure between platens is $\sigma_{z,plat} = 11.48\ f_z$, in MPa if f_z is in pN (10^{-12} N).

The platens are initially brought into contact with the crystal by applying a small $\sigma_{z,plat} = 10$ MPa and running 10^6 steps of energy minimization using the *quickmin* algorithm in LAMMPS; no dissolution nor precipitation are allowed at this point. Then, three separate simulations are run, by initially setting $\sigma_{z,plat} = 10$, 45 and 90 MPa respectively and re-equilibrating the system mechanically via 10^6 more *quickmin* steps. Then a solution with $\beta = 1$ is brought into the picture ($c_{Ca} = 16.43$ mmol/L), within a cubic simulation box of linear size 20 nm and a relatively small added solution volume $\Delta V_{sol} = 10^4$ nm^3. The crystal per se would not dissolve at $\beta = 1$, but now the applied stress is expected to induce dissolution-driven creep, with the upper platen progressively moving downward as a result. Lastly, the initial system with $\sigma_{z,plat} = 10$ MPa is immersed in a solution with $\beta = 100$ ($c_{Ca} = 92.1$ mmol/L), fixed through a $\Delta V_{sol} = 10^{24}$ nm^3; this time, the chemical drive for precipitation is expected to push up the upper platen to some extent, as an effect of crystallization pressure. In all the examples, per-particle virial stresses are computed, using each particle's volume as the averaging domain [9].

3 Results

3.1 Stress-Free Equilibrium and Dissolution/Growth of a CH Nanocrystal

Figure 3 shows the dissolution and growth of an initially spheroidal, stress-free CH nanocrystal when the surrounding aqueous solution of Ca^{2+} and OH^- ions is kept at various levels of constant saturation index β. As expected, at any $\beta < 1$ the crystal fully

dissolves; the morphology in Fig. 3c for $\beta = 0$ may actually represent an intermediate step during dissolution at any other $\beta < 1$. When $\beta = 1$ some particles precipitate but on a very long timescale, hence with very low rate. Such precipitation occurs because the rich initial morphology in Fig. 3a features possible precipitation sites which are more favourable than kink sites, hence their r_p^{net} in Eq. (8) benefits from the contribution of ΔU_d. However, when these sites are exhausted, precipitation stops and the morphology in Fig. 3b, which is just slightly more orderly than the initial one in Fig. 3a, is obtained. When $\beta > 1$ the crystal grows, but not indefinitely because that entails a high energy barrier to precipitate adatom particles on top of flat crystal surfaces; this could be achieved through a very large β, crystallography defects, or allowing for fluctuations by using the straight rates in Eqs. (2) and (6) instead of the net rates here (see [12] for more discussion on this). Within the scope of this article, Fig. 3e shows that a moderately high $\beta = 4$ (with $c_{Ca} = 27.7$ mmol/L) leads to the same small rearrangements as at $\beta = 1$, although on a much smaller timescale. At $\beta = 10$, instead, Fig. 3f shows much more precipitation and the ability to create new terrace ledges (although not new adatoms), which is sufficient to sustain significant crystallization.

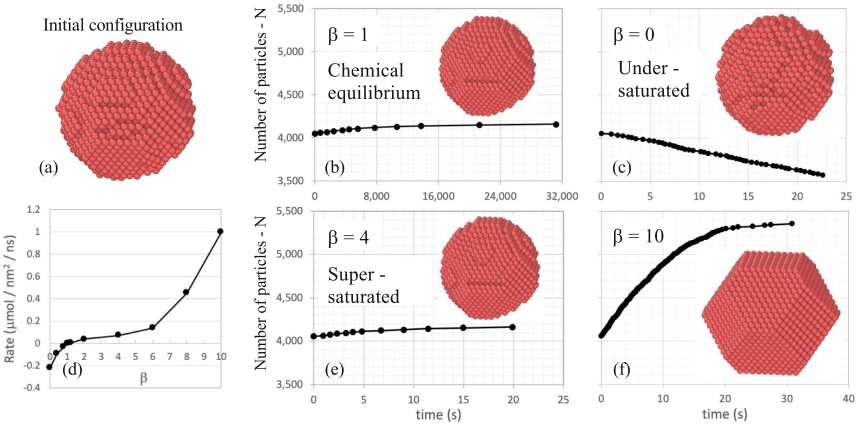

Fig. 3. (a) Initial $Ca(OH)_2$ nanocrystal. (b, c, e, f) Dissolution/precipitation at various constant saturations β, and corresponding configurations. (d) Rate vs. β curve from all the simulations.

Figure 3d gathers the rates per unit area of the crystal at all the explored β. The rates are obtained from the initial gradients of Figs. 3b, c, e, f and assuming the crystal to be a perfect sphere of known volume $N \cdot v_{m,CH}$, where N is the number of particles in a simulation at any given time. Figure 3d shows that the rate at $\beta = 1$ is negligibly small, hence chemical equilibrium is well captured. At $\beta > 1$, the inability to sustain much precipitation underlies the flattening region between $\beta = 1$ and $\beta = 6$, after which the ability to precipitate new terrace ledges and significantly grow the crystal underpins the increasing gradient of the rate vs. β curve. The significant nonlinearity of the rate curve in Fig. 3d, despite using rates derived from linear TST, stems from MASKE's ability to account for detailed morphology effects. Another strength of the KMC simulations,

evidenced in Fig. 3, is their ability to predict long timescales and realistically low rates, despite the nano length scale of the system.

3.2 Pressure-solution Creep

Figure 4 shows that a compressive stress applied to the nanocrystal, $\sigma_{z,plat}$, induces dissolution and thus a progressive reduction of the distance between platens z_t, i.e. creep from pressure solution. In all the simulations in Fig. 4, the solution is initially set to equilibrium with the solid, at $\beta = 1$. The figure also shows colour plots of the vertical stress per particle, σ_z, which is correctly greater than $\sigma_{z,plat}$ at the points of concentrated contact between crystal and platens. When a small stress is applied, in Fig. 4a, small reorganizations of the crystal surface take place with dissolution of particles near the platens immediately followed by precipitation at a small number of favourable sites. As a result, the top platen moves a bit downward, but the underlying dissolution is very slow and the solution remains near chemical equilibrium at $\beta = 1$. When more stress is applied, in Fig. 4b, the timescale of dissolution gets smaller, so creep goes faster. The solution reaches a slightly higher β, between 1 and 2, which is enough to sustain a larger downward displacement of the upper platen but no major crystallization. When an even higher stress is applied, in Fig. 4c, the timescale reduces further and β stabilizes at around 6, which Fig. 3d highlighted as a critical threshold to enable more precipitation and crystallization by forming new terrace ledges. This mechanism leads to visible crystallization in Fig. 4c and to much more dissolution and vertical displacement.

3.3 Crystallization Pressure

Figure 5 shows that setting the crystal to a high fixed $\beta = 100$ leads to widespread precipitation and crystallization, although still without the ability to create adatoms and therefore grow the crystal indefinitely. The precipitation process involves regions near the crystal-platen interfaces and is able to create sufficient vertical pressure to push upward the top platen, thus capturing qualitatively the effect of crystallization pressure. However, the current version of MASKE is likely to significantly underestimate the effect of crystallization pressure, in that the adoption of net rates and of energy minimization (instead of molecular dynamic) between discrete events of precipitation produce an averaging out of fluctuations that may add pathways for particles to squeeze in at the crystal-platen interfaces and thus further push the top platen upward.

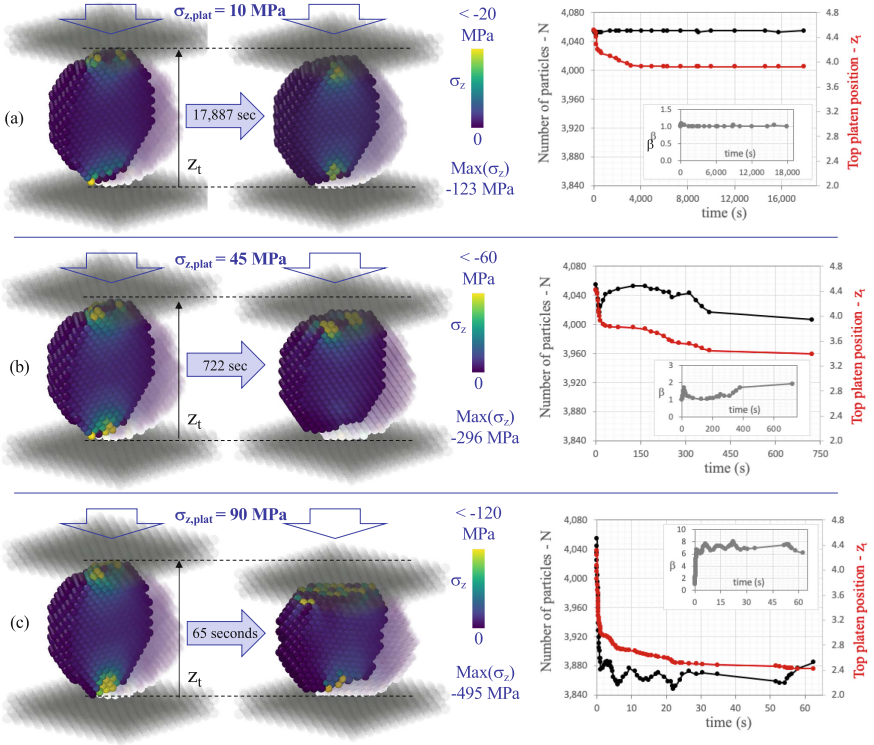

Fig. 4. Dissolution creep induced by a stress applied to the platens: (a) $\sigma_{z,plat} = 10$ MPa, (b) $\sigma_{z,plat} = 45$ MPa, (c) $\sigma_{z,plat} = 90$ MPa.

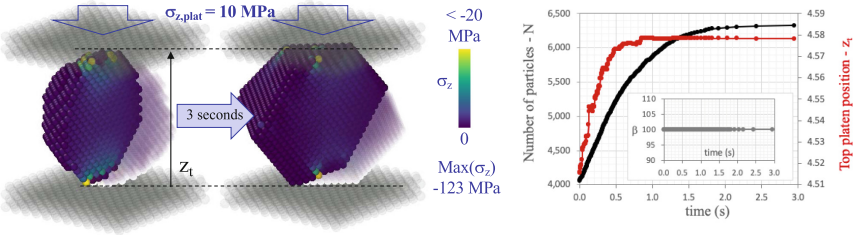

Fig. 5. Expansion from crystallization under small compression $\sigma_{z,plat} = 10$ MPa and $\beta = 100$.

4 Conclusion

The MASKE simulator is able to describe fundamental processes where chemical reactions, such as dissolution and precipitation, are coupled with mechanical stress. The simulations also predict how the morphology of reacting minerals changes during the processes. In previously published works, MASKE was already used to simulate single-phase and multi-phase processes in concrete, also including some coupling between dissolution and stress along screw dislocations.

This article has broadened the range of applications of MASKE, presenting a first set of systematic and quantitative results on creep from stress-driven dissolution, and first results on the effect of crystallization pressure. The simulations have focussed on a $Ca(OH)_2$ nanocrystal made of agglomerated particles representing one molecule each, all within a aqueous solution featuring only Ca^{2+} and OH^- ions. A number of extensions and improvements are possible now, such as studying other cement minerals (e.g. creep from solution-pressure is pronounced for gypsum), employing coarser particles each representing millions of molecules to reach larger length and time scales, and allowing for ion speciation in solution (an interface between MASKE and PHREEQC [21] is under implementation). Further extensions of MASKE are being considered too, e.g. to include ion diffusion in solution and the presence of particles representing bacteria whose metabolism also alters the solution chemistry, in particular to model self-healing concrete [22] and other bio-inspired systems for example in ground engineering [23].

Despite these possible improvements and ongoing developments, the results in this article already led to the following findings:

- The Kinetic Monte Carlo algorithm in MASKE was able to predict realistic timescales (seconds to hours) and rates, even for the nanocrystal studied here;
- Under stress-free conditions, the relationship between dissolution/growth rates and solution saturation index β is highly nonlinear, despite the rates are obtained from linear Transition State Theory. The nonlinearity stems from morphological details that MASKE captures. $\beta = 6$ emerges as a threshold level of saturation to overcome for significant crystallization to take place.
- The simulations successfully predicted creep from stress-driven dissolution, confirming that both the extent and the rate of creep can be increased by increasing the intensity of the applied stress, here from 10 to 90 MPa. The simulations of creep also confirmed that significant crystallization is triggered only when the applied stress is sufficiently large to pushes the saturation of the solution up to $\beta = 6$ threshold.
- When tested under a small stress of 10 MPa and high solution saturation $\beta = 100$, the crystal displayed some expansion which captures qualitatively the effect of crystallization pressure. However, MASKE would require additional features to describe the phenomenon of crystallization pressure in detail.

All in all, this work has shown how MASKE can simulate in detail some of the complex, fundamental processes that underpin the degradation of concrete and of other mineral systems. There is scope for similar simulations to support the development of more reliable constitutive laws for future degradation models of both traditional and new cementitious materials.

References

1. International Energy Agency: Global status report: towards a zero-emission, efficient, and resilient buildings and construction sector (2017)
2. Monteiro, P.J., Miller, S.A., Horvath, A.: Towards sustainable concrete. Nat. Mater. **16**(7), 698–699 (2017)
3. Editorial, N.: Concrete needs to lose its colossal carbon footprint. Nature **597**, 593–594 (2021)

4. Bernal, S.A., Provis, J.L., Brice, D.G., Kilcullen, A., Duxson, P., van Deventer, J.S.: Accelerated carbonation testing of alkali-activated binders significantly underestimates service life: the role of pore solution chemistry. Cem. Concr. Res. **42**(10), 1317–1326 (2012)
5. Pouhet, R., Cyr, M.: Carbonation in the pore solution of metakaolin-based geopolymer. Cem. Concr. Res. **88**, 227–235 (2016)
6. Lasaga, A.C.: Kinetic Theory in the Earth Sciences, vol. 811. Princeton University Press, Princeton (1998)
7. Pignatelli, I., Kumar, A., Alizadeh, R., Le Pape, Y., Bauchy, M., Sant, G.: A dissolution-precipitation mechanism is at the origin of concrete creep in moist environments. J. Chem. Phys. **145**(5), 054701 (2016)
8. Bažant, Z.P., Hauggaard, A.B., Baweja, S., Ulm, F.J.: Microprestress-solidification theory for concrete creep. I: aging and drying effects. J. Eng. Mech. **123**(11), 1188–1194 (1997)
9. Masoero, E., Di Luzio, G.: Nanoparticle simulations of logarithmic creep and microprestress relaxation in concrete and other disordered solids. Cem. Concr. Res. **137**, 106181 (2020)
10. Scherer, G.W.: Stress from crystallization of salt. Cem. Concr. Res. **34**(9), 1613–1624 (2004)
11. Ioannidou, K., Labbez, C., Masoero, E.: A review of coarse grained and mesoscale simulations of C–S–H. Cem. Concr. Res. **159**, 106857 (2022)
12. Shvab, I., Brochard, L., Manzano, H., Masoero, E.: Precipitation mechanisms of mesoporous nanoparticle aggregates: off-lattice, coarse-grained, kinetic simulations. Cryst. Growth Des. **17**(3), 1316–1327 (2017)
13. Coopamootoo, K., Masoero, E.: Simulations of crystal dissolution using interacting particles: prediction of stress evolution and rates at defects and application to tricalcium silicate. J. Phys. Chem. C **124**(36), 19603–19615 (2020)
14. Alex, A., Masoero, E.: Autogenous healing in cement: a kinetic Monte Carlo simulation of CaCO3 precipitation. In: Computational Modelling of Concrete and Concrete Structures, pp. 102–106. CRC Press (2022)
15. Stukowski, A.: Visualization and analysis of atomistic simulation data with OVITO–the open visualization tool. Modell. Simul. Mater. Sci. Eng. **18**(1), 015012 (2009)
16. Wittmann, F.H.: Estimation of the modulus of elasticity of calcium hydroxide. Cem. Concr. Res. **16**(6), 971–972 (1986)
17. Estrela, C., Estrela, C.R.D.A., Guimarães, L.F., Silva, R.S., Pécora, J.D.: Surface tension of calcium hydroxide associated with different substances. J. Appl. Oral Sci. **13**, 152–156 (2005)
18. Lothenbach, B., et al.: CEMDATA18: A chemical thermodynamic database for hydrated Portland cements and alkali-activated materials. Cem. Concr. Res. **115**, 472–506 (2019)
19. Domínguez, A., Jimenez, R., López-Cornejo, P., Pérez, P., Sánchez, F.: On the calculation of transition state activity coefficient and solvent effects on chemical reactions. Collect. Czech. Chem. Commun. **63**(12), 1969–1976 (1998)
20. Bullard, J.W.: A three-dimensional microstructural model of reactions and transport in aqueous mineral systems. Modell. Simul. Mater. Sci. Eng. **15**(7), 711 (2007)
21. Parkhurst, D.L., Appelo, C.A.J.: Description of input and examples for PHREEQC version 3—a computer program for speciation, batch-reaction, one-dimensional transport, and inverse geochemical calculations. US Geol. Surv. Techn. Methods **6**(A43), 497 (2013)
22. Bagga, M., et al.: Advancements in bacteria based self-healing concrete and the promise of modelling. Constr. Build. Mater. **358**, 129412 (2022)
23. Assadi-Langroudi, A., et al.: Recent advances in nature-inspired solutions for ground engineering (NiSE). Int. J. Geosynth. Ground Eng. **8**(1), 1–36 (2022)